Design and synthesis of self-ordered mesoporous nanocomposite through controlled *in-situ* crystallization

DONGLIN LI, HAOSHEN ZHOU* AND ITARU HONMA

Energy Electronics Institute, National Institute of Advanced Industrial Science and Technology (AIST), Umezono, 1-1-1, Tsukuba 305-8568, Japan
*e-mail: hs.zhou@aist.go.jp

Published online: 21 December 2003; doi:10.1038/nmat1043

Mesoporous materials are of technological interest because of their applications ranging from catalysts, molecular sieves, separation technology and gas sensors, to batteries and electronics[1–4]. Here we demonstrate a synthetic methodology that allows us to create an ordered mesoporous nanocomposite with a crystalline oxide framework. We design a 'nanocrystal–glass' configuration to build a nanoarchitecture by means of surfactant-templated self-assembly followed by the controlled *in-situ* crystallization of materials. Functional nanocrystals are used as the building blocks of ordered mesopores, and the glass phase can act both as the 'glue' between nanocrystals and as a functionalized component in the composites. Specifically, we demonstrate this methodology for ordered mesoporous nanocomposites consisting of electrochemically active nanocrystals and semiconductive glass in the TiO_2–P_2O_5–M_xO_y systems (where M is a metal ion). This approach could be applied to many other multicomponent oxides to fabricate mesoporous nanocomposites for numerous uses.

The formation of mesopores for solid oxides generally requires an amorphous framework[1], such as silica[5–8] and phosphate metal oxides[9,10], although there are a few reports of crystalline mesoporous metals[11,12]. Crystalline mesoporous oxides, which possess both ordered arrays of nanopores and a periodic atomic lattice, are desirable for many reasons. For example, many material properties depend strongly on their crystallographic constitution and especially on the periodicity over a particular length scale, typically a few nanometres. If well-defined mesopores are assembled into a crystal in a periodic array, the electrical, magnetic and optical properties of the crystal may be modified by the existence of both periodic nanopores and a periodic atomic lattice. Besides the conventional physical and chemical properties of a crystal, crystalline mesoporous solids will possess a high surface area, which is important for applications such as photocatalysis. Furthermore, nanocomposites are expected to have improved properties or combinations of properties through their connectivity or coupling of different functional components[13,14]. The assembly of ordered mesopores into an oxide nanocomposite is expected to open the possibility of designing functional mesoporous materials with additional physical and chemical properties.

However, there are enormous difficulties in synthesizing ordered mesoporous crystalline metal oxides and nanocomposites. Whereas great progress has recently been made in the synthesis of mesoporous glass-based materials such as silica and phosphate-based oxides with high thermal stability[5–10], mesostructural metal oxides have such poor thermal stability that the ordered mesostructure is easily destroyed during their production by heating[15–18]. The collapse is believed to be caused by an amorphous–crystalline transition during heating. An alternative explanation of this problem is that the structural differences between oxide glasses and metal oxides are responsible for the stability of ordered mesostructure. The glass-forming oxides, which can form a random network[19], are thermodynamically stable in an amorphous state. In contrast, the metal oxides are thermodynamically stable in a crystalline state. Inspired by glass theory[19,20], we envisaged that crystalline mesoporous nanocomposites could be developed by designing 'nanocrystal–glass' configurations. We use these not only as the building blocks of mesopores but also as the functional components

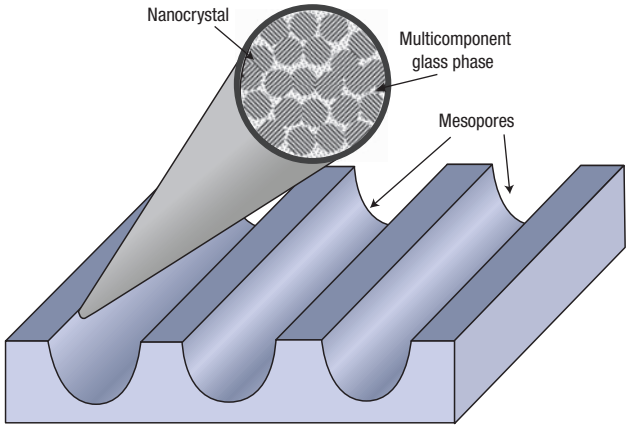

Figure 1 Target structure of designed mesoporous nanocomposite. Nanocrystal–glass configuration builds up periodic mesopores. The nanocomposite consists of a large number of nanocrystals and a smaller quantity of multicomponent glass phases.

of the composite, providing connectivity or coupling of properties such as conductivity.

The target structure of a designed mesoporous nanocomposite is shown in Fig. 1, which is similar to the 'bricks and mortar' configuration in architectural engineering (see Supplementary Information). The designed nanocomposite is made up of a large number of functional nanocrystals and smaller quantity of the multicomponent glass phase. The nanocrystals which govern the properties of the nanocomposites were designed as basic building blocks of the mesopores. The glass phase was designed to do the following: (i) provide predictable and controllable properties, because glass is a good host for most oxides; (ii) help in forming and maintaining a three-dimensional network composed of oxygen polyhedral units during molecular self-assembly; (iii) control *in-situ* crystallization of materials on a nanometre scale; (iv) form a 'glue' between the nanocrystals.

Our strategy for synthesizing such nanocomposites combines surfactant-templated self-assembly[5–10,15–18,21,22], in which ordered micelles of surfactant act as a template for the condensation of inorganic agents, with *in-situ* crystallization of glass-based nanocomposites[23–25], in which nanocrystals can precipitate within an amorphous matrix. The idea is that an organic structure-directing agent (SDA) is combined with at least two inorganic components using a sol–gel method to produce an amorphous, self-ordered, organic–inorganic hybrid. After the organic fragments have been removed from the inorganic framework through heat treatment, an amorphous inorganic solid with ordered mesopores will be produced. Subsequent heat-treatment will force desirable nanocrystals to nucleate and grow from the non-crystalline matrix, and controlling the temperature and duration of the heat-treatment determines the characteristics of the nanocrystals.

Our experiments confirmed the general idea described above. Here we select some examples to highlight the ideas involved, with an emphasis on our own work on mesoporous nanocomposites made up of nanocrystals and a glass phase. To illustrate this concept of design and synthesis of ordered mesoporous nanocomposite materials with engineered properties, we selected anatase as our functional nanocrystal. Anatase (TiO_2) has applications in photocatalysis[26], photo-cells[27,28] and electrochemical[29] devices. For the glass-forming oxide, we chose P_2O_5, which can be doped with M_xO_y (M = metal ion) to form multicomponent ionic and semiconductive conductors. This would form the 'nanocrystal/multicomponent glass' building blocks in the TiO_2–P_2O_5–M_xO_y system and provide electrochemical and semiconductive connectivity. These are expected to improve both electrochemical reaction dynamics and charge transport dynamics for lithium-inserting electrodes where reversible redox reactions involving charge transfer coupled with insertion of mobile guest lithium ions from liquid electrolyte occurs in lithium batteries. We synthesized mesostructural inorganic–surfactant hybrid gels through a surfactant-template method[15] by using a sol–gel route[23]. After being calcined at 400 °C to remove the organic template, the gels transformed into amorphous solids. Crystalline nanocomposites were produced by further heat-treating the amorphous solids at 450–700 °C, as shown in the wide-angle X-ray diffraction (WXRD) patterns of heat-treated materials (Fig. 2b).

We initially succeeded in producing the desired self-ordered mesopores in the binary TiO_2–P_2O_5 system. The powder small-angle X-ray diffraction (SXRD) patterns for the typical $75TiO_2$–$25P_2O_5$ composition of the amorphous solid calcined at 400 °C show a two-dimensional hexagonal lattice with lattice constant $a = 110$ Å in the space group *P6mm* (Fig. 2a). The as-synthesized materials containing surfactant show a similar SXRD pattern, with the somewhat larger lattice constant $a = 118$ Å (Fig. 2a inset). Transmission electron microscope (TEM) images also reveal a clear hexagonal arrangement of parallel one-dimensional channels of uniform size (see Supplementary Information), in agreement with the SXRD results. After further heat-treatment of the hexagonal mesoporous amorphous solids at 450–700 °C, the SXRD patterns also show a periodic mesostructure, although higher-order peaks become a little ambiguous with heat-

Table 1 Structure and properties of hexagonally ordered mesoporous $75TiO_2$–$25P_2O_5$ materials

Heat treatment temperatures (°C)	Active nanocrystal	Amorphous phase	Crystal size	WXRD peak intensity	SXRD $d_{(100)}$ (Å)	Pore size (nm)	BET ($m^2\ g^{-1}$)
400	amorphous	TiO_2–P_2O_5	–	no peak	95	4.7	305
450	anatase	TiO_2–P_2O_5	4.3	weak	87	4.0	308
500	anatase	TiO_2–P_2O_5	5.0	intermediate	82	4.2	290
550	anatase	TiO_2–P_2O_5	5.2	intense	78	3.9	276
600	anatase	TiO_2–P_2O_5	5.6	intense	75	3.8	203
650	anatase	TiO_2–P_2O_5	5.8	intense	77	3.3	135
700	anatase	TiO_2–P_2O_5	5.3	intense	(78)	3.5	35

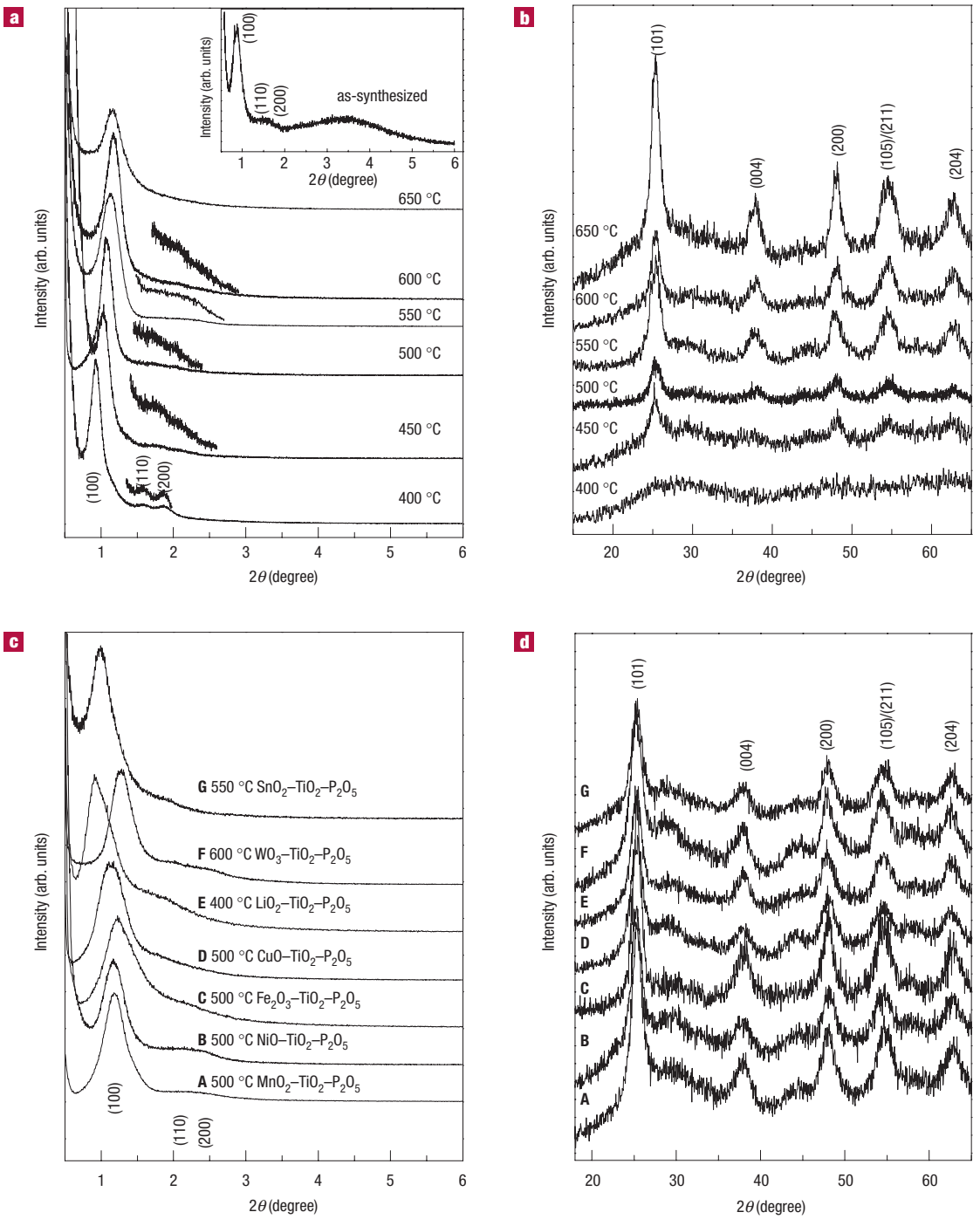

Figure 2 Powder X-ray diffraction patterns. These XRD patterns (MSA, Cu K_α, 1.54 Å) show amorphous and crystalline hexagonally ordered mesostructure (crystal is anatase). **a**, Small-angle XRD and **b**, wide-angle XRD patterns of $75TiO_2$–$25P_2O_5$ materials after heat treatment at 400, 450, 500, 550 and 650 °C; for 700 °C, see Supplementary Information. **c**, SXRD and **d**, WXRD patterns of $75TiO_2$–$20P_2O_5$–$5M_xO_y$ materials after calcination. Inset in **a** is as-synthesized material. Traces A, B, C, D, E, F and G in **c** and **d** are, respectively, SXRD and WXRD patterns for same samples.

treatment temperature (Fig. 2b). Corresponding WXRD patterns showed well-crystallized anatase peaks. The adsorption–desorption isotherms of the heat-treated samples confirm the nature of the uniform mesopores and are of type IV with a capillary condensation at relative pressure (p/p_0) ≈ 0.5–0.65 (Fig. 3). The heat-treated samples have a high surface area. Typically, the Brunauer–Emmett–Teller (BET) surface area of a sample heat-treated at 500 °C was 290 $m^2\,g^{-1}$, with a Dollimore–Head (DH) method pore diameter of 42 Å. The pore size distribution is very narrow, as shown in Fig. 3 (inset), indicating well-defined mesopores. Clearly, the original ordered mesopores maintain

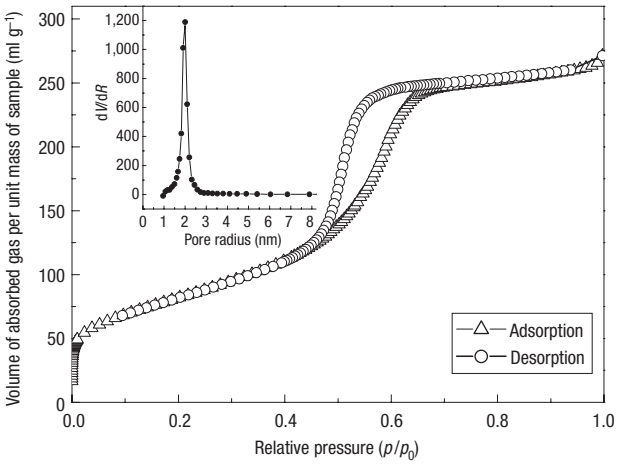

Figure 3 BET measurements. Nitrogen absorption–desorption isotherms and pore-size distribution plots (inset) for $75TiO_2$–$25P_2O_5$ nanocomposite heat treated at 500 °C, showing clear capillary condensation and narrow distribution of pore size. d*V*/d*R* is the change in adsorption volume, and d*R* is the change in radius of the pore size. The isotherms were measured using a Belsorp 18+A system. The samples were degassed for 6 hours at 150 °C before the analyses.

their structure in both amorphous and crystallized materials after heat treatment.

Table 1 summarizes the data on the structures and properties of $75TiO_2$–$25P_2O_5$ materials heat-treated under different conditions. The intensity of WXRD peaks for the crystals increases with heat-treatment temperature whereas the average size of the crystals is stable below 6 nm. Meanwhile, the d_{100} spacing in the SXRD patterns decreases with heat-treatment temperature, 87 Å for 450 °C and 75 Å for 600 °C, which indicates that the walls of the pores were condensed owing to the shrinkage of the materials.

Most of the crystallized materials showed a uniform pore size in TEM images (Fig. 4a). At higher magnification, the TEM images reveal close and dense lattice fringes of crystals in the framework of well-defined mesopores (Fig. 4b). High-resolution TEM images clearly show both nanocrystals and an amorphous phase (Fig. 4c). Elemental analysis from spatially resolved energy dispersive spectroscopy (EDS) confirms the coexistence of two phases, a crystalline phase with TiO_2 composition and an amorphous phase composed of titanium, phosphorus and oxygen (see Supplementary Information). After examining samples heat-treated at different temperatures, we found the following. (i) As in the usual sol–gel-derived titania, nanocrystals easily nucleate within an amorphous matrix. (ii) A large number of TiO_2 nanocrystals are assembled together through a small quantity of titanophosphate glass phases, building up a wall of ordered mesopores. (iii) At heat-treatment temperatures of 450–650 °C, the amount of the crystal increases with temperature, whereas crystal size stabilizes in the range of 3–8 nm, with no abnormally large crystals observed, in agreement with the XRD data (Table 1). We thus conclude that the nanometre-scale crystals build up the whole framework of ordered mesopores, forming a well-defined mesoporous nanocomposite composed of dense uniform-sized anatase nanocrystals and a small quantity of P_2O_5–TiO_2 glass phases.

To control the crystallization behaviour, it is important to add other metal oxides with the special properties needed to compose the glass phase. Here, we modified the binary TiO_2–P_2O_5 system by adding into 5–10% (molar ratio) of several metal oxides, ranging from monovalent to hexavalent, such as Li_2O, CuO, NiO, Fe_2O_3, MnO_2, SnO_2 and WO_3. The systems containing Li_2O, NiO and CuO easily crystallized at lower temperature. In contrast, WO_3 hindered crystallization of the materials. For example, a TiO_2–P_2O_5–Li_2O system crystallized at 350–400 °C, whereas a TiO_2–P_2O_5–WO_3 system of similar composition began to crystallize at 600 °C. Multicomponent $75TiO_2$–$20P_2O_5$–$5M_xO_y$ materials showed an ordered mesostructure (Fig. 2c; Fig. 3d, e), and crystals grown from these multicomponent amorphous solids were also anatase (Fig. 2d). It is worth noting that the density of nanocrystals in

Table 2 Structure and desirable properties of hexagonally ordered mesoporous $75TiO_2$–$20P_2O_5$–$5M_xO_y$ materials*

Material systems	Active nanocrystal	Amorphous phase	Crystal size (nm)	Pore size (nm)	BET ($m^2\ g^{-1}$)	T_s (°C)	T_c (°C)	Glass properties	Composite properties
LiTiPO	anatase	TiO_2–P_2O_5–Li_2O	4.9	3.9	195	400	450	Ionic conductor; electrochemistry	Electrochemistry, photo-catalysis
NiTiPO	anatase	TiO_2–P_2O_5–NiO	5.7	3.9	208	500	550	Semiconductor; electrochemistry	Electrochemistry, photo-catalysis
CuTiPO	anatase	TiO_2–P_2O_5–CuO	5.0	4.1	306	500	550	Semiconductor; electrochemistry	Electrochemistry; photo-catalysis
FeTiPO	anatase	TiO_2–P_2O_5–Fe_2O_3	4.6	4.5	257	500	650	Semiconductor; electrochemistry	Electrochemistry; photo-catalysis
MnTiPO	anatase	TiO_2–P_2O_5–MnO_2	5.7	4.5	271	500	600	Semiconductor; electrochemistry	Electrochemistry; photo-catalysis
SnTiPO	anatase	TiO_2–P_2O_5–SnO_2	5.3	3.3	232	550	650	Semiconductor; electrochemistry	Electrochemistry; photo-catalysis
WTiPO	anatase	TiO_2–P_2O_5–WO_3	5.3	4.3	230	600	700	Semiconductor electrochemistry	Electrochemistry; photo-catalysis

*All samples were heat treated at 400 °C for 6 hours to remove organic agencies, then annealed at T_s temperatures for 1 hour.

T_s, starting temperature of crystallization evaluated from XRD patterns. T_c, the collapse temperature of the most ordered mesophase evaluated from XRD patterns.

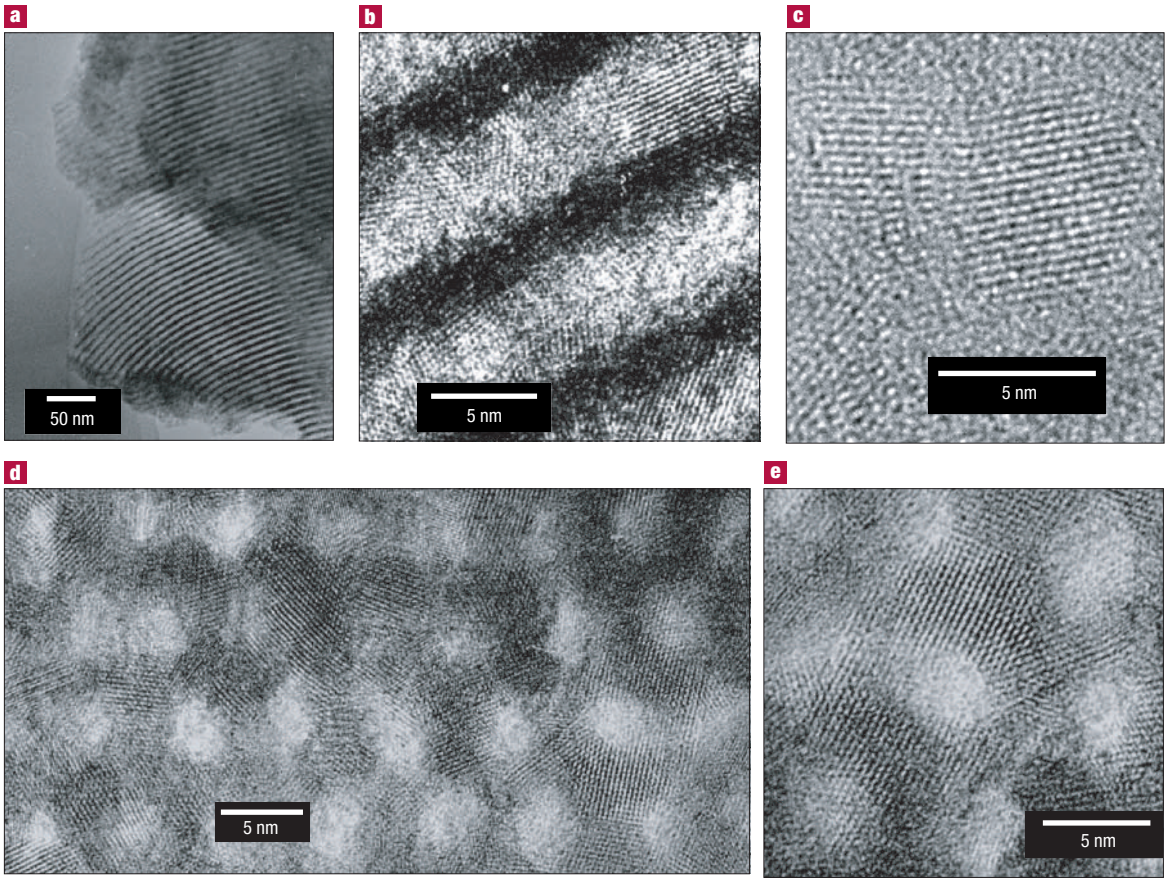

Figure 4 Representative TEM images. The microscope is a JEOL 1200EX operating at 200 kV. **a**, Uniform [110]-oriented channels in the nanocomposite derived from a sample heat-treated at 500 °C. **b**, Magnified view of **a**, showing dense lattice fringes of nanocrystals in parallel channels. **c**, HRTEM image of **a**, showing configuration of nanocrystals and amorphous phase. **d**, Hexagonal mesopores oriented along [001] with crystalline framework in $75TiO_2$–$20P_2O_5$–$5MnO_2$ nanocomposite heat-treated at 500 °C. **e**, HRTEM image of **d**, showing mesoporous anatase crystallites building up the hexagonal mesoporous framework.

heat-treated multicomponent systems was higher and their sizes more uniform (Fig. 4d) than those in the binary TiO_2–P_2O_5 system. In particular, many larger well-crystallized crystals with curved surfaces constituted the walls of the ordered mesopores (Fig. 4d, e). These curved surfaces indicate that the original mesostructure was maintained after crystallization, and that mesopores can form across well-crystallized TiO_2.

In addition to helping to stabilize the ordered mesoporous configuration, the multicomponent glass phase can impart physical properties to the mesopore framework. For electrochemical and mesoscopically conductive properties of the composites, we introduced 5–10 mol% M_xO_y with ionic conductivity or semiconductivity into the binary TiO_2–P_2O_5 system, as described above. These oxides are incorporated into the titanophosphate glass to form an ionically conductive or semiconductive glass phase. Combining the electrochemically active, but conductively poor, TiO_2 with an ionically conductive or semiconductive TiO_2–P_2O_5–M_xO_y glass on the nanoscale in the mesopore walls should improve the electrochemical reactivity of the nanocomposites, and improve the transport of charge carriers resulting from electrochemical reaction.

This kind of nanocomposite has high thermal stability (see Tables 1 and 2). For heat treatments in the range 400–600 °C, the nanocomposites have a BET surface area of more than 200 $m^2\,g^{-1}$. Even up to 650 °C, they retain a surface area of more than 100 $m^2\,g^{-1}$. As the heat-treatment temperatures are increased up to 700 °C, partially ordered mesopores with a DH pore diameter of 35 Å still remain (see Supplementary Information), although most of the mesopores collapse, resulting in a surface area of 35 $m^2\,g^{-1}$. By contrast, the ordered mesostructure in surfactant-templated pure TiO_2 is completely destroyed after crystallization above 400 °C, although it may show a BET surface area of more than 100 $m^2\,g^{-1}$. A high thermal stability makes the walls of the mesopores sinter and increase in density on heat-treatment. As a consequence, there might be an opportunity for fabricating mesoporous ceramics through the sintering process in ceramics technology.

The above measurements show that we have successfully synthesized a hexagonal mesoporous nanocomposite with a crystalline framework. The nanocomposite reported here differs from all previous works on mesoporous oxides[5–10,15–18]. Most of the previous studies on mesoporous materials have been on glass-forming oxides, which form an amorphous inorganic framework; some studies on mesoporous single-component metal oxides[15] have reported a few nanocrystals of ~3 nm, a 'semicrystalline' framework. In our work, a large number of well-crystallized nanocrystal 'building blocks' and a small quantity of glass phase 'glues' build up highly ordered mesopores. To our knowledge, Figs 2 and 4

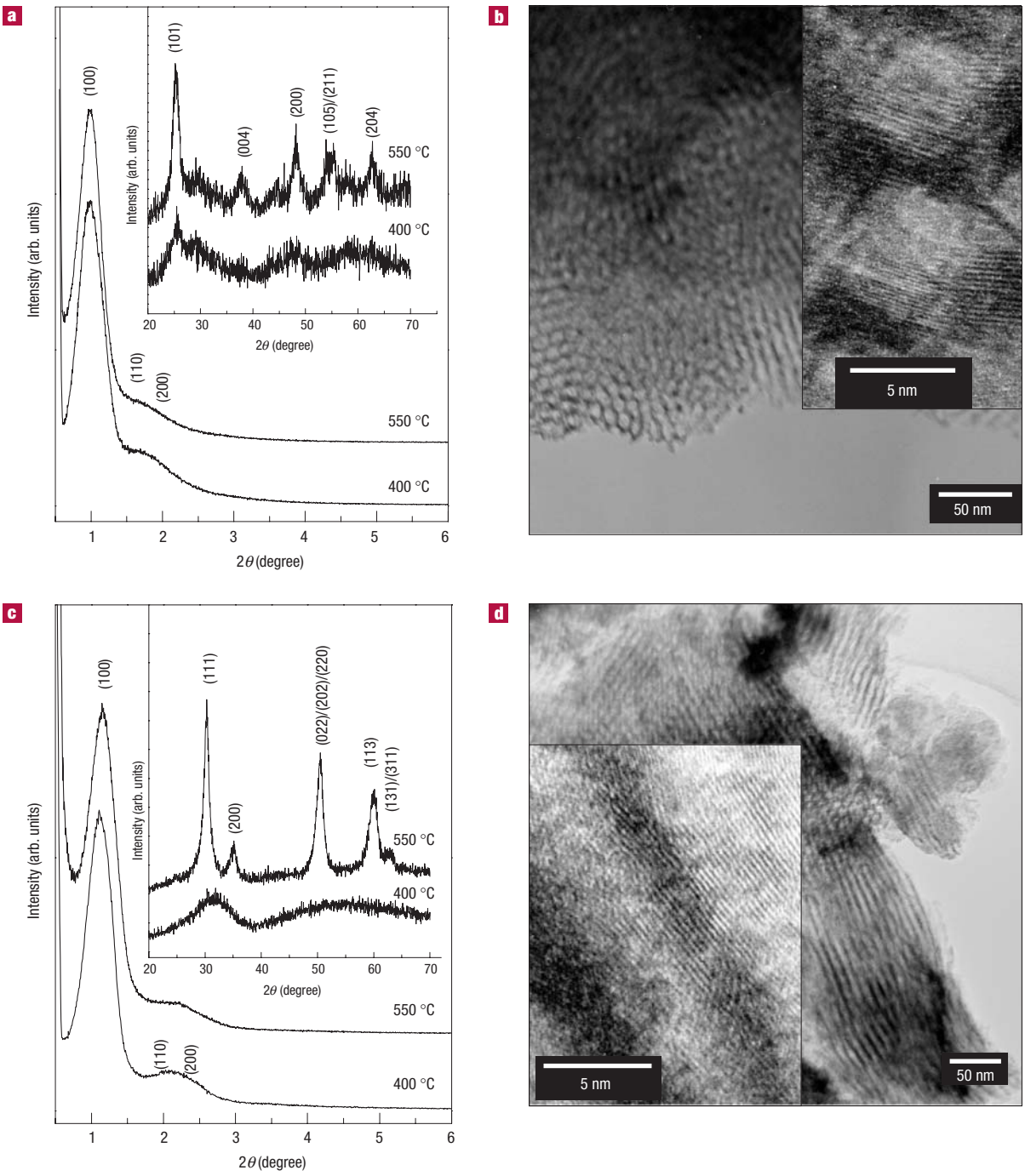

Figure 5 Powder X-ray diffraction patterns and TEM images. a, SXRD and (inset) WXRD patterns (MSA, Cu K_{α}, 1.54 Å) of $80TiO_2$–$20SiO_2$ materials calcined at 400 °C and 550 °C , and **b**, TEM images of just the sample heat treated at 550 °C along the [001] direction. Samples heat treated at 550 °C show crystalline hexagonal mesostructure built from anatase nanocrystals. **c**, Small and wide-angle XRD patterns of $80ZrO$–$20P_2O_5$ materials heat treated at 400 °C and 550 °C, and **d**, TEM images of just the sample heat treated at 550 °C along the [100] direction. Again, samples heat treated at 550 °C show crystalline hexagonal mesostructure built from anatase nanocrystals. In TEM images, HRTEM (inset) images show clear lattice fringes of the crystals that build up ordered mesopores.

show the first example of periodic arrays of ordered mesopores or nanotubes of metal oxide nanocomposites consisting predominantly of nanocrystals.

One of the advantages of our work is that adding a small quantity of a multicomponent glass phase allows us to combine the merits of self-assembly of organic–inorganic hybrids with traditional crystallization technology, and thus to design and synthesize crystalline mesoporous materials with predetermined properties. More importantly, mesoporous composite structures such as these may show connectivity properties or integrate different functions.

We now consider the possibility that the wall of the ordered mesopores is in fact made up of anatase nanocrystals precipitating from the mesoporous multicomponent amorphous solid through *in-situ* crystallization. Generally, crystallization is divided into three different stages: nucleation, growth and coarsening. Because amorphous metal oxides are thermodynamically metastable at elevated temperature, crystallization is unavoidable for these oxides during heat treatment. In the case of single-component, sol–gel-derived TiO_2, the amorphous-to-anatase transition occurs at 400–450 °C (ref. 30). Subsequent heat-treatment at higher temperature will give rise to coarsening of the nanocrystals. Large crystals tend to grow and small ones to shrink and finally dissolve. During coarsening, a large number of nanocrystals grow into larger crystals by consuming small ones. Because all nanocrystals are randomly oriented in space, the coarsening of nanocrystals is random and disordered on scales larger than the pore diameter (from tens of nanometres to submicrometre). This kind of random coarsening of nanocrystals will destroy the ordered mesophase composted of ordered nanopores with a wall of 3–6 nm thickness. Adding a small amount of glass-forming oxide to the metal oxides will modify both the structure and crystallization characteristics of materials. In the TiO_2–P_2O_5 ($0 < P/Ti < 1$) system, phosphate anions, [PO_4], are homogeneously dispersed in the amorphous TiO_2 matrix, forming solid hetero-networks composed of both tetrahedral PO_4 and octahedral TiO_6 groups[31]. This heterostructure easily produces phase separation on a nanoscale, forming both nano-sized P-rich phases and P-poor phases (TiO_2 phase) during heat treatment. Anatase nuclei in the TiO_2 phase easily nucleate because they have the same structural unit, a [TiO_6] octahedron, as amorphous TiO_2. In fact, a large number of nuclei were observed in the TEM observations of amorphous TiO_2–P_2O_5. Further heat treatment makes the TiO_2 nuclei grow into nanocrystals by consuming the amorphous TiO_2 phase produced from continuous phase separation. Accompanying the nucleation and growth of anatase crystals, the residual amorphous phase gradually becomes P-rich, resulting in a stable titanophosphate glass phase. A thermodynamically stable glass phase prevents the mass diffusion of Ti ions for further growth of nanocrystals, thus resulting in a stable structure. The random coarsening of nanocrystals, which would destroy the ordered mesostructure, is hindered. As a result, the nanocrystal–glass composite preserves the original ordered mesostructure at high temperature.

In TiO_2–P_2O_5–M_xO_y systems, 5 mol% of M_xO_y is incorporated into the glass phase, forming multicomponent titanophosphate glass. Low-valence oxides such as Li_2O, NiO and CuO result in non-bridging oxygen bonds, breaking the glass network, and WO_3 tends to form bridging oxygen bonds to be incorporated into glass network. The former increase the crystallization tendency, and the latter hinders crystallization (Table 2). The power of the glass phase to control crystallization is, therefore, its ability to control simultaneously the microenvironment of nucleation and the growth of crystals. We infer, therefore, that a 'nanocrystal–glass' configuation makes it possible to control many of the crucial aspects of mesoporous metal oxides through the crystallization of materials, instead of preventing crystallization.

We anticipate that this 'nanocrystal–glass' building block can be applied to other metal oxides as a general approach. In fact, a number of crystalline mesoporous nanocomposites can be designed and synthesized by selecting different nanocrystals and glass phases. Using silica as a glass-forming oxide, we have also synthesized an ordered mesoporous anatase-based nanocomposite in the TiO_2–SiO_2 system. Figure 5a and b shows XRD patterns and TEM images of hexagonal ordered mesoporous nanocomposites of typical composition $80TiO_2$–$20SiO_2$. For this material, anatase nanocrystals begin to precipitate at 550 °C, and the original ordered mesostructure remains up to 700 °C. Other nanocrystals can also be substituted: for example, using ZrO_2 as the crystalline phase, we have synthesized a well-crystallized hexagonal mesoporous ZrO_2-based nanocomposite in a ZrO_2–P_2O_5 system (Fig. 5c and d). The average size of orthorhombic ZrO_2 crystallites is about 10 nm, based on XRD measurement. In the HRTEM observation of $80ZrO_2$–$20P_2O_5$ materials, the lattice fringes of ZrO_2 often extend across two mesopores, thus confirming the existence of mesoporous crystals (Fig. 5d, inset). Ordered mesoporous TiO_2–SiO_2 and ZrO_2–P_2O_5 nanocomposites show a BET specific surface area of 100–300 $m^2\,g^{-1}$. Furthermore, the crystallization temperature and thermal stability of SiO_2-based materials increase with SiO_2 content, which makes it possible to design and synthesize thermally stable mesoporous SiO_2-based nanocomposites. In addition, disordered porous nanocrystal-based composites have been synthesized in the oxide systems of ZrO_2–SiO_2, TiO_2–P_2O_5–SiO_2, ZrO_2–P_2O_5–SiO_2, Nb_2O_5–P_2O_5, Nb_2O_5–SiO_2, WO_3–P_2O_5 and WO_3–SiO_2 (D.L. *et al.*, unpublished results). These nanocrystal-based composites can be easily doped with alkali-metal or alkaline-earth oxides, and an extensive class of nanocomposites will be derived for different applications through the doping of functional components.

The use of a crystal–glass configuration as a building block allows the design and synthesis of mesoporous nanocomposites with desirable properties. Because of high thermal stability, our approach is applicable to a wide range of compositions. Combining this with molecular self-assembly and heat-treatment processes means that the physical and chemical properties of mesoporous, nanocrystal-based nanocomposites can be varied in a controlled manner, which has an important bearing on their practical use. Also, this kind of nanocrystal–glass building block can be seen as an important step towards almost fully crystalline mesoporous materials. Such a mesoporous structure is not easily accessible with single-component metallic oxides[15–18].

METHODS

The starting materials for inorganic precursors were $Ti(OC_3H_7)_3$, $PO(OC_2H_5)_3$, $Zr(OC_4H_9)_4$, $Si(OC_2H_5)_4$, PCl_3, $NbCl_5$, LiCl, $NiCl_2$, $FeCl_3$, $CuCl_2$, $MnCl_2$, $SnCl_4$ and WCl_5. The tri-block copolymer $HO(CH_2CH_2O)_{20}(CH_2CH(CH_3)O)_{70}(CH_2CH_2O)_{20}H((EO)_{20}(PO)_{70}(EO)_{20}$; Pluronic P–123, BASF) was used as the surfactant template.

In a typical synthesis, 0.8–1.2 g of P123 was dissolved in 8–10 g of ethanol (EtOH). To this solution, 2.5 g of $Ti(OC_3H_7)_3$ was added and the mixture was stirred for 10 min, forming a transparent solution in the presence of 0.6 g 0.5N HCl. We then added 1–2 g of $PO(C_2H_5)_3$ to this solution. In the case of doped materials, 5–10 mol% of metal chloride was added with stirring. The multicomponent mixtures were stirred in a sealed bottle for 20 hours. After the transparent sols had been gelled in an open Petri dish at room temperature in air for 5 days, the resulting transparent gel was dried at 80 °C for 7 days in an oven. The as-synthesized samples were heat treated at 400 °C for 6 hours to remove organic species, forming inorganic amorphous solids. Subsequently, the products were heat-treated at 400–700 °C for 1–2 hours in air, producing the desired nanocomposites.

Received 9 July 2003; accepted 24 November 2003; published 21 December 2003.

References

1. Davis, M. E. Ordered porous materials for emerging applications. *Nature* **417,** 813–821 (2002).
2. Yamata, T. *et al.* Surface photo voltage NO gas sensing properties dependent on the structure of self ordered mesoporous silicate film. *Adv. Mater.* **14,** 812–815 (2002).
3. Kavan, L., Rathousky, J., Gratzel, M., Shklover, V. & Zukal, A. Mesoporous thin film TiO_2 electrodes. *Micro. Meso. Mater.* **44–45,** 653–659 (2001).
4. Miller, R. D. In search of low-k dielectrics. *Science* **286,** 421–423 (1999).
5. Kresge, C. T., Leonowicz, M. E., Roth, W. J., Vartuli, J. C. & Beck, J. S. Ordered mesoporous molecular sieves synthesized by a liquid-crystal template mechanism. *Nature* **359,** 710–712 (1992).
6. Attard, G. S., Glyde, J. C. & Goltner, C. G. Liquid-crystalline phases as templates for the synthesis of mesoporous silica. *Nature* **378,** 366–378 (1995).
7. Zhao, D. *et al.* Triblock copolymer syntheses of mesoporous silica with periodic 50 to 300 angstrom pores. *Science* **279,** 548–552 (1998).
8. Templin, M. *et al.* Organically modified aluminosilicate mesostructures from block copolymer phases. *Science* **278,** 1795–1798 (1997).
9. Bhaumik, A. & Inagaki, S. Mesoporous titanium phosphate molecular sieves with ion-exchange capacity. *J. Am. Chem. Soc.* **123,** 691–696 (2001).
10. Tian, B. *et al.* Self-adjusted synthesis of ordered stable mesoporous minerals by acid–base pairs. *Nature Mater.* **2,** 159–163 (2003).
11 Attard, G. S. *et al. Science* **278,** 838–841 (1997).
12. Bartlett, P. N., Birkin, P. N., Ghanem, M. A., de Groot, P. & Sawicki, M. The electrochemical deposition of nanostructured Ccobalt film from lyotropic liquid crystalline media. *J. Electrochem. Soc.* **148,** C119–C123 (2001).
13. Tressler, J. F., Alkoy, S., Dogan, A. & Newnham, R. E. Functional composites for sensors, actuators and transducers. *Composites A* **30,** 477–482 (1997).
14. Zen, H., Li, J., Liu, J. P., Wang, Z. L. & Sun, S. Exchange-coupled nanocomposite magnets by nanoparticle self-assembly. *Nature* **420,** 395–398 (2002).